18

Maximizing Local Access to Therapeutic Deliveries in Glioblastoma. Part II: Arborizing Catheter for Convection-Enhanced Delivery in Tissue Phantoms

EGLEIDE Y. ELENES[1] • CHRISTOPHER G. RYLANDER[1,2]

[1]Department of Biomedical Engineering, The University of Texas at Austin, TX, USA; [2]Department of Mechanical Engineering, The University of Texas at Austin, TX, USA

Author for correspondence: Christopher Rylander, Department of Mechanical Engineering, The University of Texas at Austin, 204 E. Dean Keeton Street, Stop C2200, Austin, TX 78712-1591, USA. E-mail: cgr@austin.utexas.edu

Doi: http://dx.doi.org/10.15586/codon.glioblastoma.2017.ch18

Abstract: Convection-enhanced delivery (CED) is the process of local, pressure-driven flow of drugs into brain parenchyma containing tumor tissue, resulting in greater distribution of the infused drugs compared to diffusion-dependent therapies. Nevertheless, even with the advantage of CED over simple diffusion, the large volumes necessary to target entire tumors and peritumor volumes have been previously unachievable with currently available catheters. We present a novel, multiport, arborizing catheter designed specifically for improving drug distribution into the brain. We evaluated the performance of the arborizing catheter by quantifying volume dispersed (V_d) and mean distribution ratios (V_d:V_i) in infusion studies

In: *Glioblastoma*. Steven De Vleeschouwer (Editor), Codon Publications, Brisbane, Australia
ISBN: 978-0-9944381-2-6; Doi: http://dx.doi.org/10.15586/codon.glioblastoma.2017

using agarose brain phantoms and compared results to a single-port catheter. Three experimental groups were evaluated: (i) single-port infusions at 1 μL/min; (ii) single-port infusions at 7 μL/min; and (iii) seven-port arborizing catheter infusions at 1 μL/min/port. Significantly greater V_d was calculated for the arborizing catheter group (10.47 ± 1.07 cm^3) compared with the single-port catheter groups at the low- and high-flow rates (2.36 ± 0.21 cm^3 and 5.14 ± 0.56 cm^3), respectively. V_d:V_i for the arborizing catheter was 37% lower than the single-port catheter at 1 μL/min, but 100% greater than the single-port catheter at 7 μL/min. The multiport, arborizing catheter produced the greatest distribution of the infusate, which would be advantageous for CED; however, it did not exhibit the greatest distribution ratio, likely due to overlapping distribution volumes from the multiple individual ports.

Key words: Blood–brain barrier; Catheters; Convection-enhanced delivery; Glioblastoma; Infusate

Introduction

Distribution of therapeutic agents within the central nervous system (CNS) is limited and challenging with existing drug delivery techniques. Systemic delivery of drugs is nontargeted and has been associated with systemic toxicity. Furthermore, the blood–brain barrier (BBB) hinders drugs from reaching the CNS in sufficient quantities (1). Technologies such as catheters and pumps, intrathecal injections, and drug-impregnated polymers are challenged by interstitial fluid pressure and are limited to the diffusivity and molecular weight of the therapeutic. In an effort to address the challenges of current drug-delivery methods, convection-enhanced delivery (CED) was pioneered at the National Institute of Neurological Disorders and Stroke, as an alternate approach to deliver large concentrations of macromolecules directly into the brain parenchyma, effectively circumventing the BBB (2, 3). CED permits local delivery of high-molecular weight molecules via a small-caliber catheter inserted through a burr hole created in the skull and dura. This technique relies on pressure-driven bulk flow of the fluid that is pushed primarily through the interstitial space, achieving high concentrations of the infusate, distributed centimeters into the tissue, an order of magnitude greater than with diffusion alone (2, 4). Moreover, CED per se does not lead to cerebral edema and is unaffected by capillary loss or metabolism of the macromolecule (5). With these initial studies, CED was established as a viable method for providing regional distribution of large molecules, such as proteins and some conventional chemotherapeutic agents, in the brain (6–9). Compared with other therapies, CED minimizes systemic and CNS toxicity by local delivery of high concentrations of therapeutics directly to the brain tissue and has led to treatment applications in several cerebral disorders, including Parkinson's (10, 11), epilepsy (12), Alzheimer's (13, 14), and malignant gliomas (4, 5, 15–21).

Although distribution of macromolecules is more effective with CED than with diffusion-based therapies and positive results in pre-clinical and early clinical trials for malignant gliomas (7, 8, 18, 22–24) showed promise of this technique,

progress toward clinical translation has been challenged by inadequate results in high-profile, Phase III clinical trials (16). The PRECISE trial was a study of the experimental drug IL13-PE38QQR, a tumor-targeting agent made by combining the human protein IL13 with a portion of the bacterial toxin *Pseudomonas* exotoxin, which was continuously infused directly into the brain for treatment in adult patients with glioblastoma at first recurrence. Retrospective investigations of the study's results have revealed that overly ambitious study endpoints, inaccurate catheter positioning, and poor drug distribution are likely explanations behind the PRECISE trial's failure to meet clinical endpoints (25). Sampson et al. estimated that, on average, only approximately 20% of the 2-cm tumor margins surrounding the resection cavity were covered with the therapeutic (25). The inability of CED to perfuse drugs over large volumes, including margins beyond the primary enhancing tumor detected by magnetic resonance imaging, is highly problematic as these margins contain infiltrative malignant cells that may be responsible for regrowth of the tumor.

Arborizing Catheter for CED in Tissue Phantoms

OPTIMIZATION OF CATHETERS USED FOR CED

In light of the results of various clinical trials, researchers have turned to examine whether the available technology used to perform CED is suited to overcome the unique challenges hindering drug distribution in the brain. The anatomical heterogeneity of the brain and tumor tissue, differences in permeability between white and gray matter, and issues arising from low-pressure "sinks," such as cerebrospinal fluid spaces, can all inhibit drug distribution with CED. Specifically, the design of the catheters used to perform the infusions has undergone scrutiny (26–29). In the PRECISE trial, investigators performed the treatment using commercially available catheters designed for different medical applications. Similarly, various other CED studies have been limited by the "off-label-use" of various commercial catheters that may not possess the capability to effectively perfuse drugs over large tissue volumes (Table 1). In order to achieve targeted delivery and infuse greater tumor volumes, CED often requires insertions of multiple catheters, thus increasing the risk of trauma to healthy neurological tissue and increasing the probability of seeding malignant cells in healthy tissue along the needle tract. Thus, researchers have begun to investigate using catheters that offer multiple ports of infusion originating from a single insertion tract (Cleveland Multiport Catheter™, Infuseon Therapeutics, Inc.) (30). Others have opted for a different approach and are investigating chronic delivery of therapeutics using catheters that are permanently implanted, and accessed via a port on the side of the cranium (31). Another common drawback of CED is reflux of drug along the insertion tract, which results in ineffective drug distribution and premature termination of the CED therapy. Reflux-arresting properties have been investigated and incorporated in the design of catheters such as a "step change," in which the diameter of the catheter changes drastically along the distal tip of the catheter, which has shown to mitigate reflux during CED (26, 27, 32–34).

It is our hypothesis that addressing the challenge of poor drug distribution can potentially improve the success of CED. Here, we present the design and

TABLE 1 Catheters Used in CED Studies

Catheter	Company	Study
Barium-impregnated one-port infusion catheter	Medtronic® PS Medical (Goleta, CA, USA)	Phase I/II (35)
Barium-impregnated one-port infusion catheter	Vygon US LLC (Valley Forge, PA, USA)	Phase III (PRECISE) (36)
Reflux-preventing neuro-ventricular cannula	SmartFlow® MRI Interventions (Irvine, CA, USA)	Phase I (37)
Cleveland Multiport Catheter™	Infuseon Therapeutics, Inc (Cleveland, OH, USA)	Early Phase I (30)

evaluation of an arborizing catheter that enhances dispersal of the infusate. Once the arborizing catheter is inserted into the skull, individual microneedles can be deployed, arborizing from a single cannula, providing multiple infusion ports per one primary cannula insertion tract. These individual microneedles can be positioned independently, at various insertion depths, to control the location of infusion. Upon completion of the therapy, the microneedles can be fully retracted back into the cannula; thus, the tumor-contacting surfaces of needles would remain completely shielded within the primary cannula, reducing the probability of tumor cell-seeding in healthy brain tissue and preventing mechanical damage to surrounding tissue when extracting the catheter. Furthermore, the arborizing catheter has an inherent step change at the interface between the microneedles and the primary cannula to help reduce the occurrence of reflux during the infusion. We hypothesize that with multiple, separated infusion ports, the arborizing catheter will achieve greater volumetric dispersal of the infusate and greater mean distribution ratio (volume dispersed to the total volume infused), compared to a single-port catheter.

ARBORIZING CATHETER DESIGN AND MANUFACTURING

Early-stage prototypes for the arborizing catheter (Figure 1A, B) consisted of a primary cannula with an outer diameter of 3 mm (38). The cannula was manufactured by bonding seven aligned biocompatible polyether ether ketone (PEEK) tubes (41568-L4, Analytical Sales & Services; OD 794 µm × ID 381 µm) with a light-cured medical grade adhesive (3972, Loctite®). At the distal end of the cannula, the PEEK tubes were twisted using a custom-designed fixture. The twist at the end of the cannula caused the microneedles to branch out at an angle of up to 20° (angle of peripheral needles from cannula axis) when they were deployed. Once the adhesive was cured, the distal end of the cannula was polished to a smooth conical tip (Figure 1B). The cannula was made to house seven microneedles made from flexible, hollow silica optical fibers (TSP180375, General Separation Technologies) (OD 375 µm × ID 180 µm) polished to a smooth bevel tip (Figure 1C). The distal end of each microneedle was attached

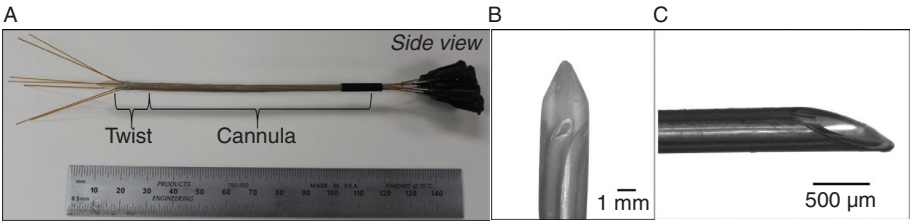

Figure 1 Images of the arborizing catheter prototype. (**A**) Side view of the arborizing catheter with deployed microneedles at the distal end of the cannula (left) where the twisted PEEK tubing is labeled. At the proximal end of the cannula (right), the proximal end of the microneedles is shown with attached Luer lock adapters. (**B**) Magnified image showing twisted PEAK tubing at distal end of the cannula, which allowed microneedle deflection. (**C**) Magnified image of a polished, bevel-tipped microneedle.

to a 22G hypodermic needle with a Luer lock adapter to allow for easy connection to small bore extension tubing. When deploying the microneedles, the small diameter of the needles compared to the primary cannula created a step change that helped arrest reflux as demonstrated in other catheters with an incorporated step change (32, 34).

MANUFACTURING OF SINGLE-PORT MICRONEEDLE CATHETER

We manufactured single-port catheters in order to test our hypothesis and compare the performance of the single-port catheter versus the arborizing catheter prototypes in infusion studies. The single-port catheter consisted of a single microneedle (OD 375 µm × ID 180 µm), 3 cm in length, attached to a 22 G hypodermic needle (0.75 in. length) with a Luer lock. The distal end of the single-port catheter was polished to a smooth bevel tip.

EVALUATION OF ARBORIZING CATHETER PROTOTYPE IN TISSUE PHANTOMS

Agarose tissue phantoms were prepared for infusion studies. An agarose solution was mixed at 0.6% (w/w) by reconstituting agarose powder in deionized water. The solution was heated to a low boil and continuously stirred until all the agarose powder was completely mixed. The agarose was allowed to cool at room temperature and then poured into transparent molds. For all experiments, the agarose solution was decanted into the mold, and the device of interest (single or arborizing catheter) was inserted in the solution while still liquid (approximately at 50°C). This casting method allowed a tight seal around the device and helped mitigate reflux. The agarose was allowed to set at room temperature and infusion began when the temperature of the agarose reached 23 ± 2°C. For infusions using a single microneedle, a polystyrene mold (1.7 cm × 8.1 cm × 3.9 cm) with an open top was used, and for infusions using an arborizing catheter, a 10-cm cubic glass mold was used.

The goal of this study was to compare the volume dispersed and mean distribution ratio for a given infusion using a single-port catheter versus the arborizing

catheter, which is a multiport catheter consisting of seven microneedles. Using a programmable pump (PHD ULTRA™ Syringe Pump, Harvard Apparatus) to control volumetric flow rate, 5% (w/w) indigo carmine dye was infused in the agarose gel. As a baseline, the V_d and V_d:V_i for a single-port catheter was determined at a flow rate of 1 µL/min for 100 min. The mean distribution ratio (V_d:V_i) was calculated by dividing the V_d by the total infused volume (V_i) that was programmed in the syringe pump. A similar infusion was performed using the arborizing catheter. The flow rate for each microneedle was kept at 1 µL/min/needle. Finally, because the arborizing catheter consists of seven microneedles, each a delivery port, a third set of infusions was performed using a single-port catheter with seven times higher flow rate in order to compare V_d and V_d:V_i when equal volumes of infusate were delivered to the tissue phantom (i.e., equivalent to the V_i for the arborizing catheter). To summarize, the three experimental groups were: (i) single-port infusions (n = 5) at a flow rate of 1 µL/min for a total V_i of 100 µL; (ii) single-port infusions (n = 5) at a flow rate of 7 µL/min for a total V_i of 700 µL, and (iii) infusion with the arborizing catheter (n = 5) performed at 1 µL/min/needle for a total V_i of 700 µL.

To evaluate the prototypes, a shadowgraphy experimental setup was used consisting of a clear stage with reflecting mirrors on the left side and bottom (Figure 2). For each infusion, the sample was placed on the stage and backlit

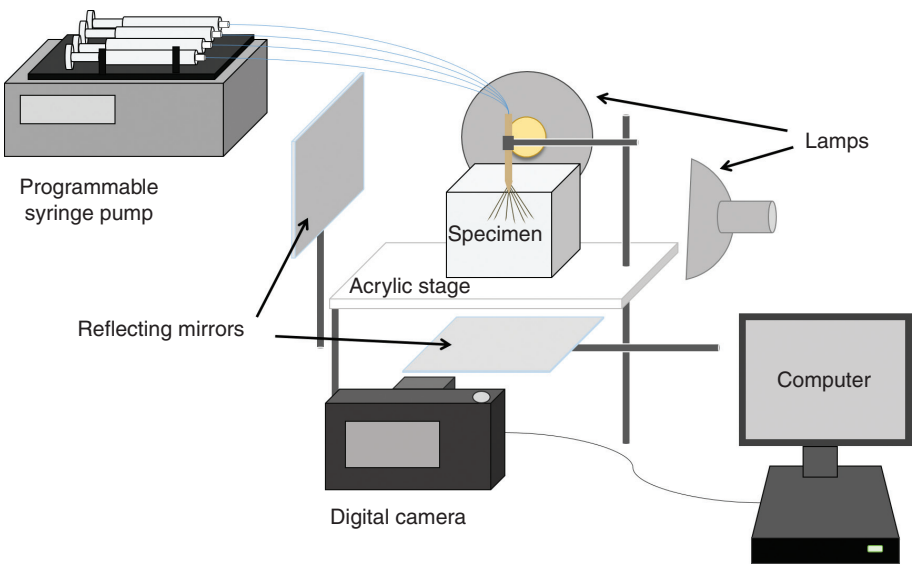

Figure 2 Shadowgraphy experimental setup. A programmable syringe pump is used to control the infusion of indigo carmine dye into agarose tissue phantoms placed on a clear acrylic stage backlit by lamps placed behind a light-diffusing sheet (not shown) to minimize variations in light intensity in each of the three views. A DSLR camera controlled by a desktop computer captures images of all three views (front view captured directly by the camera, and side and bottom views reflected to the camera by the angled mirrors) at a rate of one frame per minute.

with various lamps placed behind a light-diffusing sheet. A DSLR camera (Rebel T1i, Cannon), mounted in front of the stage, simultaneously captured images containing three views of the sample (front, side, and bottom), within the same frame, which were used to estimate the volume dispersed of the infused dye. Images were captured at a rate of one frame per minute for a total of 100 min. Metric scale bars were included in each image.

The images were then processed using an algorithm coded in Matlab (Mathworks, Natick, MA). Original images were cropped into three separate view frames: front, side, and bottom. Each cropped frame was then subtracted from the first image in the series to remove the background and thus only show the infusion volume. The differential images were converted to grayscale and then to binary images using image processing functions on Matlab that compute a global threshold value using Otsu's method (39). Pixels with intensity values below the threshold value were assigned black and pixels with intensity values greater than the threshold value were assigned white.

The volume dispersed for each cropped view frame was quantified using an image processing method previously described (40). Briefly, the method assumes that V_d is axisymmetric about the axis of single-port catheter or primary cannula of the arborizing catheter. The volume is discretized into elementary frustums of right circular cones. The algorithm counts the number of black pixels in each discretized section to calculate the bottom and top diameters of each frustum. A scale factor, extracted from the original image, was used to scale the pixel sizes of each binary image. The final volume was calculated by summing the volume of all the individual frustums. The final V_d for an infusion was reported as the average of the three views (front, side, and bottom) of each image. The mean distribution ratio was calculated by dividing the V_d by the total volume (V_i) that was programmed in the syringe pump. For infusions using the single-port catheter, the volume was observed to be relatively spherical. Therefore, only the front view of the images was used to calculate V_d.

Using the statistical software R (R Foundation for Statistical Computing, Vienna, Austria), one-way ANOVA tests were performed to analyze differences in V_d and V_d:V_i for the three experimental groups assuming a significance level of 0.05. A Tukey–Kramer test was performed for pairwise comparisons among the three experimental groups.

ADVANTAGE OF SEVEN PORTS VERSUS SINGLE PORT

Results for volume dispersed and mean distribution ratio using a single-port catheter at 1 μL/min for 100 min were 2.36 cm^3 and 23.61, respectively (Figure 3). When the flow rate for the single-port catheter was increased sevenfold, the V_d increased by only approximately 117.7% to 5.14 cm^3, and V_d:V_i decreased by approximately 69% to 7.34. However, comparisons of V_d and V_d:V_i using the arborizing catheter show that we can achieve a V_d of 10.47 cm^3 and V_d:V_i of 14.95 with our current catheter prototype. Compared to the single-port catheter at 7 μL/min, the values for V_d and V_d:V_i achieved with the arborizing catheter were two times greater. It is important to note that the total V_i, across all microneedles in the arborizing catheter, was the same for the arborizing catheter and the single-port catheter at a 7 μL/min flow rate experimental groups. This suggests that the

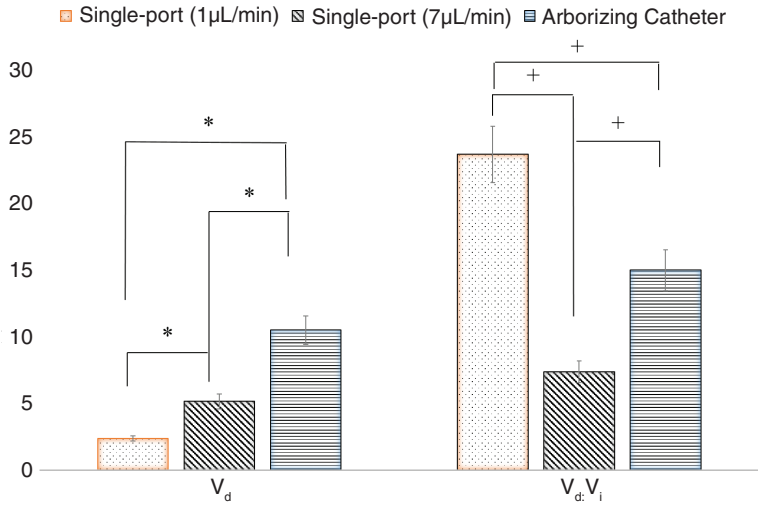

Figure 3 Statistical comparisons of average volume dispersed and mean distribution ratio results. A one-way ANOVA test was performed to analyze differences in average volume dispersed (V_d in cm^3) and average mean distribution ratios (V_d:V_i) after 100 min of continuous infusion in agarose tissue phantoms for the three experimental groups: (i) single-port catheter at a flow rate of 1 μL/min; (ii) single-port infusions at a flow rate of 7 μL/min; (iii) arborizing catheter. A Tukey–Kramer test was performed for pairwise comparisons. Values for V_d were significantly different when each group was compared (*$P < 0.001$). Similarly, values for V_d:Vi were significantly different from each other among the three groups (+ $P < 0.0001$).

arborizing catheter can achieve significantly ($P < 0.001$) greater volumetric dispersal of the infusate, when it is distributed among seven microneedles instead of coming out of a single port. This would be beneficial in CED because it is desirable to distribute the therapeutic agent throughout the entire tumor volume, including the surrounding tumor margins, in order to completely target any infiltrative malignant cells.

A visual representation of V_d for the three groups can be seen in Figure 4. In these binary images taken at the final time point of the infusion for each experimental group, the greater V_d achieved with the arborizing catheter can be appreciated. For this sample, the V_d of 12.13 cm^3 obtained after 100 min is equivalent to coverage of a spherical volume with a 2.8-cm radius. The single-port catheter at the slower flow rate (1 μL/min) resulted in the lowest V_d value. This is expected because the overall V_i for that group was seven times lower than for the single-port catheter at the higher flow rate (7 μL/min) and for the arborizing catheter groups. However, it can be appreciated that even though the total infused volume for the single-port group at the highest flow rate (7 μL/min) and the arborizing catheter were the same, the resultant volume dispersed was greater for the arborizing catheter.

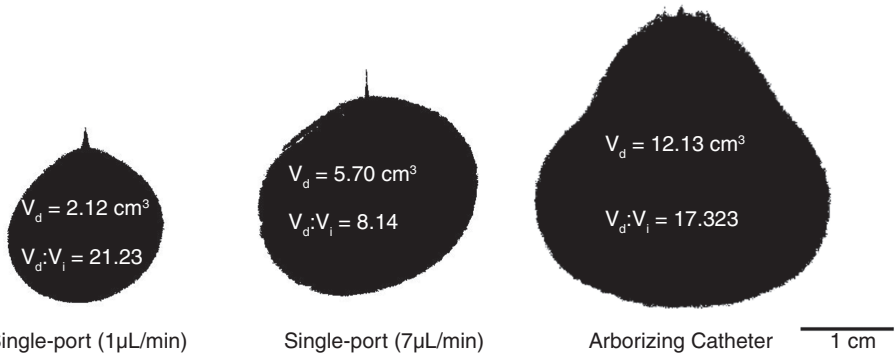

Figure 4 Representative volume dispersed for each experimental group after 100 min of continuous infusion. All images are of the front view captured directly by the DSLR camera. The volume dispersed (V_d) and mean distribution ratios (V_d:V_i) were calculated using an algorithm that discretizes the volume into elementary frustums of right circular cones (40). The final volume is calculated by summing the volumes of all the frustums.

V_d:V_I VERSUS TIME INDICATES OVERLAP IN THE INFUSION DISTRIBUTION

Although the single-port catheter (1 μL/min) group showed the lowest V_d, it resulted in the highest V_d:V_i of the three groups. In comparison to the arborizing catheter group, the catheter is composed of seven microneedles, with each individual microneedle representing a single port (each at a flow rate of 1 μL/min). However, at the end of the 100-min-long infusion, the overall V_d:V_i for all the microneedles of the arborizing catheter resulted in an approximately 37% lower mean distribution ratio compared to single-port catheter at the slower flow rate (1 μL/min). The V_d:V_i over time is shown in Figure 5 for the three experimental groups. The V_d:V_i for the arborizing catheter group is similar to that of the single port at the slower infusion rate of 1 μL/min; however, it begins to decline and eventually becomes lower than the single-port (1 μL/min) group by 60 min of continuous infusion. This could be explained by the likely overlap in the local infusions from individual microneedles as they become larger with time. It is likely that at the beginning of the infusion, the overlap of the individual volume provided by each needle is less pronounced, therefore the V_d:V_i is similar to that of the single-port catheter. However, as the volumes dispersed from individual needles become bigger and merge with one another into one large volume, the benefit gained from the multiple ports in the arborizing catheter is reduced until eventually the V_d:V_i becomes less than that of a single-port catheter. The single-port (7 μL/min) group, which has the lowest V_d:V_i, further supports the concept of overlap. The infused dye, concentrated in a smaller volume, resulted in mean distribution ratios that plateau quickly during the infusion and stayed relatively constant after approximately 20 min of continuous infusion. We observed that, once deployed, the separation distance of the individual microneedles of the arborizing catheter affects the amount of overlap between the local infusions of

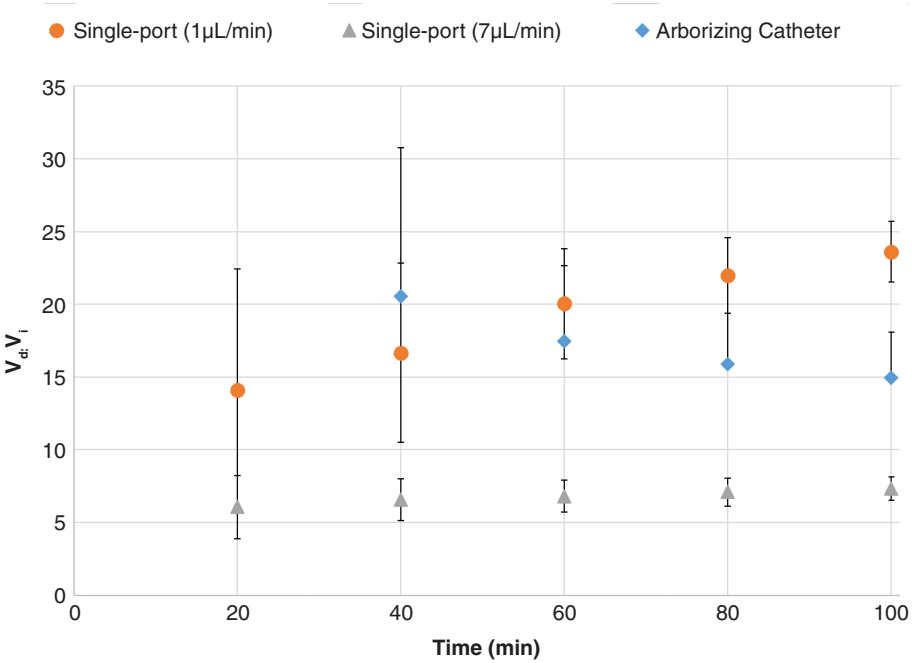

Figure 5 Mean distribution ratios (V_d:V_i) versus time of infusions for the three experimental groups. The average V_d:V_i for each group was calculated every 20 min. However, the image processing algorithm was limited to calculating volume of solid, axisymmetric shapes and could not reliably calculate the volume of infusion shapes with gaps or holes. Therefore, infusions in the arborizing catheter group were calculated at 40 min and beyond, after the infusion shapes of individual microneedles had overlapped sufficiently to form a solid shape.

each microneedle and influences the measured V_d. In future iterations of the arborizing catheter prototype, we will optimize the catheter design to increase the angle of deflection of the microneedles, so that we can minimize the amount of overlap in the V_d of individual needles and maximize V_d:V_i for the arborizing catheter.

It is important to note that our image processing algorithm was not able to reliably calculate V_d for the arborizing catheter at time points less than 40 min. This is because we assumed that the infusion volume was axisymmetric about the axis of the primary cannula of the arborizing catheter and thus, it was not able to account for any amorphous shapes or holes in the infusion volume. Figure 6 shows binary images of three representative time points in the infusion of an arborizing catheter. After 10 min of continuous infusion, the dispersed volume from individual microneedles is clearly discernible. At 20 min, there are still gaps present in the volume dispersed. However, after 40 min, most gaps in the volume dispersed had been filled and a reliable calculation for V_d could be obtained.

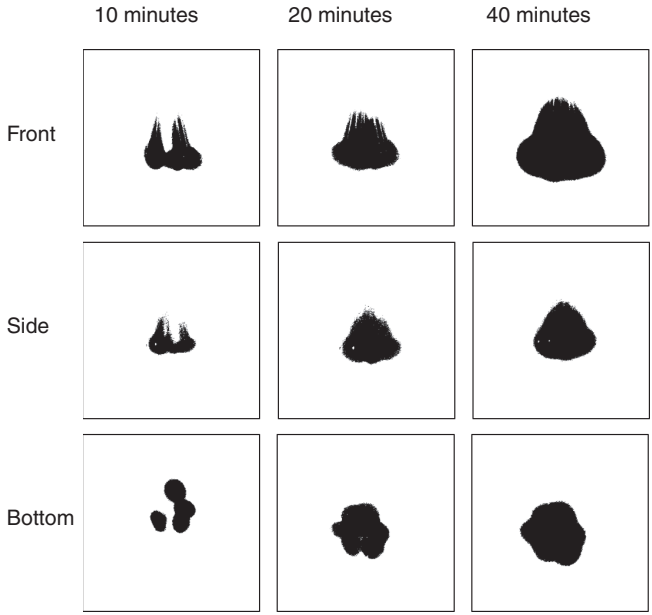

Figure 6 Representative binary images of volume dispersed for the arborizing catheter at three time points during the infusion for three view frames. The images show that at time points below 40 min, there were gaps in the dispersed volume due to branching out of the microneedles in the arborizing catheter. As the individual infusion volumes from each microneedle grew and began overlapping each other, the gaps were filled.

Conclusion

Results indicate that the multiport, arborizing catheter can significantly enhance volumetric dispersal of the infusate over a single port. By separating the volume infused, the arborizing catheter achieved a twofold greater volumetric dispersal and mean distribution volume compared to a single-port catheter for the same total infused volume. When comparing infusions of the arborizing catheter to that of a single-port catheter at the same flow rate per microneedle, the mean distribution ratio for the arborizing catheter drops to approximately 37% less than the single-port, perhaps due to overlap in the individual volume dispersed in the seven microneedles of the catheter. In the next design iteration, separation of individual microneedles within the arborizing catheter will be optimized to minimize overlap in the infusion volumes of individual microneedles (but, with no gaps in between them), while maximizing volumetric dispersal.

Acknowledgment: Portions of this chapter were supported by grants from the Wallace H. Coulter Foundation, National Science Foundation NSF/CBET 0933571, National Institutes of Health NIH/NCI R21CA156078, and the Virginia Center for Innovative Technology Commonwealth Research Commercialization Fund.

The author would like to thank the following institutions and collaborators for their contributions to the generation of data and material support of experiments presented in this section:

- Wake Forest University Comprehensive Cancer Center and Brain Tumor Center of Excellence: Dr. Waldemar Debinski and Dr. Stephen Tatter
- Virginia Tech-Wake Forest University School of Biomedical Engineering and Sciences: Dr. John Rossmeisl, Dr. John Robertson, and Dr. David Grant

Conflict of Interest: Arborizing catheter and fiberoptic microneedle device fabrication methods and applications are described in US Patent 8,798,722, issued on August 5, 2014, and US Application 14/002,058, both of which are managed by the Virginia Tech Intellectual Properties (VTIP) Group.

References

1. Patel MM, Goyal BR, Bhadada SV, Bhatt JS, Amin AF. Getting into the brain: Approaches to enhance brain drug delivery. CNS Drugs. 2009 Feb;23(1):35–58. https://doi.org/10.2165/0023210-200923010-00003
2. Bobo RH, Laske DW, Akbasak A, Morrison PF, Dedrick RL, Oldfield EH. Convection-enhanced delivery of macromolecules in the brain. Proc Natl Acad Sci U S A. 1994 March;91:2076–80. https://doi.org/10.1073/pnas.91.6.2076
3. Morrison PF, Laske DW, Bobo H, Oldfield EH, Dedrick RL. High-flow microinfusion: Tissue penetration and pharmacodynamics. Am J Physiol. 1994 Jan;266(1 Pt 2):R292–305. https://doi.org/10.1007/978-3-7091-8592-6_58
4. Bosch DA, Hindmarsch T, Larsson S, Backlund EO. Intraneoplastic administration of bleomycin in intracerebral gliomas: A pilot study. In: Gillingham F, Gybels J, Hitchcock E, Rossi G, Szikla G, editors. Advances in stereotactic and functional neurosurgery 4. Acta Neurochirurgica Supplementum. 30. Vienna: Springer; 1980. p. 441–4.
5. Vandergrift WA, Patel SJ, Nicholas JS, Varma AK. Convection-enhanced delivery of immunotoxins and radioisotopes for treatment of malignant gliomas. Neurosurg Focus. 2006 April;20(4):E13. https://doi.org/10.3171/foc.2006.20.4.8
6. Degen JW, Walbridge S, Vortmeyer AO, Oldfield EH, Lonser RR. Safety and efficacy of convection-enhanced delivery of gemcitabine or carboplatin in a malignant glioma model in rats. J Neurosurg. 2003 Nov;99(5):893–8. https://doi.org/10.3171/jns.2003.99.5.0893
7. Kunwar S. Convection enhanced delivery of IL13-PE38QQR for treatment of recurrent malignant glioma: Presentation of interim findings from ongoing phase 1 studies. Acta Neurochir Suppl. 2003 Feb;88:105–11. https://doi.org/10.1007/978-3-7091-6090-9_16
8. Laske DW, Youle RJ, Oldfield EH. Tumor regression with regional distribution of the targeted toxin TF-CRM107 in patients with malignant brain tumors. Nat Med. 1997 Dec;3:1362–8. https://doi.org/10.1038/nm1297-1362
9. Lieberman DM, Laske DW, Morrison PF, Bankiewicz KS, Oldfield EH. Convection-enhanced distribution of large molecules in gray matter during interstitial drug infusion. J Neurosurg. 1995 Jun;82:1021–9. https://doi.org/10.3171/jns.1995.82.6.1021

10. Gill SS, Patel NK, Hotton GR, O'Sullivan K, McCarter R, Bunnage M, et al. Direct brain infusion of glial cell line-derived neurotrophic factor in Parkinson disease. Nat Med. 2003 May;9(5):589–95. https://doi.org/10.1038/nm850
11. Slevin JT, Gerhardt GA, Smith CD, Gash DM, Kryscio R, Young B. Improvement of bilaterial motor functions in patients with Parkinson disease through the uniteral intraputaminal infsion of glial cell line-derived neurotrophic factor. J Neurosug. 2005 Feb;102:216–22. https://doi.org/10.3171/jns.2005.102.2.0216
12. Rogawski MA. Convection-enhanced delivery in the treatment of epilepsy. Neurotherapeutics. 2009 Apr;6(2):344–51.
13. Barua NU, Miners JS, Bienemann AS, Wyatt MJ, Welser K, Tabor AB, et al. Convection-enhanced delivery of neprilysin: A novel amyloid-β-degrading therapeutic strategy. J Alzheimers Dis. 2012;32(1):43–56. https://doi.org/10.3233/JAD-2012-120658
14. Miners JS, Barua N, Kehoe PG, Gill S, Love S. AB-degrading enzymes: Potential for treatment of alzheimer disease. J Neuropathol Exp Neurol. 2011 Nov;70(11):944–59. https://doi.org/10.1097/NEN.0b013e3182345e46
15. Sampson JH, Brady ML, Petry NA, Croteau D, Friedman AH, Friedman HS, et al. Intracerebral infusate distribution by convection-enhanced delivery in humans with malignant gliomas: Descriptive effects of target anatomy and catheter positioning. Neurosurgery. 2007 Feb;90(2):89–99. https://doi.org/10.1227/01.NEU.0000249256.09289.5F
16. Kunwar S, Chang S, Westphal M, Vogelbaum M, Sampson J, Barnett G, et al. Phase III randomized trial of CED of IL13-PE38QQR vs gliadel wafers for recurrent glioblastoma. Neuro Oncol. 2010 Aug;12(8):871–81. https://doi.org/10.1093/neuonc/nop054
17. Debinski W, Tatter SB. Convection-enhanced delivery for the treatment of brain tumors. Expert Rev Neurother. 2009 Oct;9(10):1519–27. https://doi.org/10.1586/ern.09.99
18. Lidar Z, Mardor Y, Jonas T, Pfeffer R, Faibel M, Nass D, et al. Convection-enhanced delivery of paclitaxel for the treatment of recurrent malignant glioma: A phase I/II clinical study. J Neurosurg. 2004 Mar;100(3):472–9. https://doi.org/10.3171/jns.2004.100.3.0472
19. Yang W, Huo T, Barth RF, Gupta N, Weldon M, Grecula JC, et al. Convection enhanced delivery of carboplatin in combination with radiotherapy for the treatment of brain tumors. J Neurooncol. 2011 Feb;101(3):379–90. https://doi.org/10.1007/s11060-010-0272-z
20. Vogelbaum MA, Aghi MK. Convection-enhanced delivery for the treatment of glioblastoma. Neuro Oncol. 2015 Mar;17 Suppl 2:ii3–ii8. https://doi.org/10.1093/neuonc/nou354
21. Patchell RA, Regine WF, Ashton P, Tibbs PA, Wilson D, Shappley D, et al. A phase I trial of continuously infused intratumoral bleomycin for the treatment of recurrent glioblastoma multiforme. J Neurooncol. 2002 Oct;60(1):37–42. https://doi.org/10.1023/A:1020291229317
22. Patel SJ, Shapiro WR, Laske DW, Jensen RL, Asher AL, Wessels BW, et al. Safety and feasibility of convection-enhanced delivery of cotara for the treatment of malignant glioma: Initial experience in 51 patients. Neurosurgery. 2005 June;56(6):1243–53. https://doi.org/10.1227/01.NEU.0000159649.71890.30
23. Rand RW, Kreitman RJ, Patronas N, Varricchio F, Pastan I, Puri RK. Intratumoral administration of recombinant circularly permuted interleukin-4-pseudonomas exotoxin in patients with high-grade glioma. Clin Cancer Res. 2010 Jun;6:2157–65.
24. Sampson JH, Akabani G, Archer GE, Bigner DD, Berger MS, Friedman AH, et al. Progress report of a phase I study of the intracerebral microinfusion of a recombinant chimeric protein composed of transforming growth factor (TGF)-α and a mutated form of the Pseudomonas exotoxin termed PE-38 (TP-38) for the treatment of malignant brain tumors. J Neurooncol. 2003 Nov;65(1):27–35. https://doi.org/10.1023/A:1026290315809
25. Sampson JH, Archer G, Pedain C, Wembacher-Schroder E, Westphal M, Kunwar S, et al. Poor drug distribution as a possible explanation for the results of the PRECISE trial. J Neurosurg. 2010 Aug;113(2):301–9. https://doi.org/10.3171/2009.11.JNS091052
26. Brady ML, Raghavan R, Singh D, Anand PJ, Fleisher AS, Mata J, et al. In vivo performance of a microfabricated catheter for intraparenchymal delivery. J Neurosci Meth. 2014 May 30;229:76–83. https://doi.org/10.1016/j.jneumeth.2014.03.016

27. Gill T, Barua NU, Woolley M, Bienemann AS, Johnson DE, Sullivan SO, et al. In vitro and in vivo testing of a novel recessed-step catheter for reflux-free convection-enhanced drug delivery to the brain. J Neurosci Meth. 2013 Sep 30;219(1):1–9. https://doi.org/10.1016/j.jneumeth.2013.06.008
28. Seunguk O, Odland R, Wilson SR, Kroeger KM, Liu C, Lowenstein PR, et al. Improved distribution of small molecules and viral vectors in the murine brain using a hollow fiber catheter. J Neurosurg. 2007 Sep;107(3):568–77. https://doi.org/10.3171/JNS-07/09/0568
29. Olson JJ, Zhang Z, Dillehay D, Stubbs J. Assessment of a balloon-tipped catheter modified for intracerebral convection-enhanced delivery. J Neurooncol. 2008 Sep;89(2):159–68. https://doi.org/10.1007/s11060-008-9612-7
30. Vogelbaum M. A pilot trial of intraparenchymally-administered topotecan using Convection-Enhanced Delivery (CED) in patients with suspected recurrent/progressive WHO grade III or IV (High Grade) glioma requiring stereotactic biopsy. In: ClinicalTrialsgov. Bethesda, MD: National Library of Medicine (US). NLM Indentifier: NCT02278510; 2014.
31. Barua NU, Hopkins K, Woolley M, O'Sullivan K, Harrison R, Edwards RJ, et al. A novel implantable catheter system with transcutaneous port for intermitten convection-enhanced delivery of carboplatin for recurrent glioblastoma. Drug Delivery. 2016;23(1):17–173. https://doi.org/10.3109/10717544.2014.908248
32. Krauze MT, Saito R, Noble C, Tamas M, Bringas J, Park JW, et al. Reflux-free cannula for convection-enhanced high-speed delivery of therapeutic agents. J Neurosurg. 2005 Nov;103(5):923–9. https://doi.org/10.3171/jns.2005.103.5.0923
33. Vazquez LC, Hagel E, Willenberg BJ, Dai W, Casanova F, Batich CD, et al. Polymer-coated cannulas for the reduction of backflow during intraparenchymal infusions. J Mater Sci Mater Med. 2012 Aug;23(8):2037–46. https://doi.org/10.1007/s10856-012-4652-0
34. Yin D, Forsayeth J, Bankiewicz KS. Optimized cannula design and placement for convection-enhanced delivery in rat striatum. J Neurosci Meth. 2010 Mar 15;187(1):46–51. https://doi.org/10.1016/j.jneumeth.2009.12.008
35. Andriani RT. Design and validation of medical devices for photothermally augmented treatments [MS Thesis]. Blacksburg, VA: Virginia Tech; 2014.
36. Otsu N. A threshold selection method from gray-level histograms. IEEE Trans Syst Man Cyb. 1975 Jun;9(1):62–6. https://doi.org/10.1109/TSMC.1979.4310076
37. Sabliov CM, Boldor D, Keener KM, Farkas BE. Image processing method to determine surface area and volume of axi-symmetric agricultural products. Int J Food Prop. 2002 Jan;5(3):641–53. https://doi.org/10.1081/JFP-120015498
38. Mut M, Sherman JH, Shaffrey ME, Schiff D. Cintredekin besudotox in treatment of malignant glioma. Expert Opin Biol Th. 2008;8(6):805–12.
39. Mueller S, Polley MY, Lee B, Kunwar S, Pedain C, Wembacher-Schroder E, et al. Effect of imaging and catheter characteristics on clinical outcome for patients in the PRECISE study. J Neurooncol. 2011 Jan;101(2):267–77. https://doi.org/10.1007/s11060-010-0255-0
40. Tocagen. A phase 1 ascending dose trial of the safety and tolerability of toca 511 in patients with recurrent high grade glioma. In: ClinicalTrialsgov [Internet]. Bethesda, MD: National Library of Medicine (US). NLM Identifier: NCT01156584; 2010.